Bound and free surface waves in a large wind-wave tank

William J. Plant and Peter H. Dahl
Applied Physics Laboratory, University of Washington, Seattle, Washington, USA

Jean-Paul Giovanangeli and Hubert Branger
Institut de Recherche sur les Phénomènes Hors Équilibre, Centre National de la Recherche Scientifique, Marseille, France

Received 23 February 2004; revised 3 June 2004; accepted 28 June 2004; published 5 October 2004.

[1] Microwave and acoustic systems operated in the large wind-wave tank in Luminy, Marseille, France, show that most small-scale waves produced at large angles to the wind are products of breaking events bound to longer waves in the tank. These longer waves propagate at the dominant wave phase speed for fetches near 7 m but travel at speeds corresponding to the phase speed of a wave half as long as the dominant wave at fetches near 26 m. The microwave and acoustic systems operated at both 8 mm and 2 cm wavelengths. They were set to look at the same surface spot simultaneously at the same incidence and azimuth angles. Measurements were made at seven wind speeds, five incidence angles, seven azimuth angles, and two nominal fetches. Two peaks were found in either the microwave or acoustic Doppler spectrum when looking upwind or downwind but never in both. The low-frequency peak is due to Bragg scattering from freely propagating short waves, while the high-frequency peak is a result of Bragg scattering from short waves bound to longer waves. At azimuth angles not aligned with the wind direction the high-frequency peak was found to move lower until it merged with the low-frequency peak at azimuth angles around 60°. Fitting the first moments of these Doppler spectra along with the backscattering cross sections to a model of free wave/bound wave scattering showed that the intensity of bound and free short waves generally decreased with azimuth angle but that free wave spectral densities decreased more rapidly. Differences in microwave and acoustic cross sections confirmed that the bound waves were tilted by their parent waves. Spectral densities of bound and free waves were estimated individually by fitting the data to the model. The sum of these spectral densities, the total short-wave spectral density, was similar to, but lower than, previous measurements. The nature of millimeter-length bound waves was found to be different at long fetches than at short fetches, a feature not observed in centimeter-length bound waves. *INDEX TERMS:* 6969 Radio Science: Remote sensing; 6959 Radio Science: Radio oceanography; 4504 Oceanography: Physical: Air/sea interactions (0312); 4506 Oceanography: Physical: Capillary waves; *KEYWORDS:* sea return, bound waves, ocean surface waves

Citation: Plant, W. J., P. H. Dahl, J.-P. Giovanangeli, and H. Branger (2004), Bound and free surface waves in a large wind-wave tank, *J. Geophys. Res.*, *109*, C10002, doi:10.1029/2004JC002342.

1. Bound and Free Surface Waves

[2] For several years, investigations have shown that not all short surface waves on wind-roughened water surfaces are generated directly by the wind [*Hara et al.*, 1997; *Plant*, 1997; *Fedorov et al.*, 1998; *Plant et al.*, 1999a, 1999b; *Rozenberg et al.*, 1999; *Plant*, 2003a, 2003b]. Rather, a significant fraction (up to 50%) of short surface waves with lengths in the centimeter and millimeter range are generated by longer waves through distortions, through the production of parasitic capillary waves, or through breaking [*Plant et al.*, 1999a; *Plant*, 2003a]. Here we designate free waves to be short waves directly generated by the wind and bound waves to be those generated by longer waves. Bound waves are, in general, given a mean tilt by their parent waves and move at speeds near those of their parent waves, which are often much faster than their intrinsic phase speed.

[3] While these past studies have determined the existence of bound and free waves on wind-roughened water surfaces, they have been unable to determine the angular dependence of bound and free waves separately. Furthermore, past studies have shown that bound waves travel at the speed of the dominant wave in tanks with fetches of 15 m or less, while on the ocean they travel at speeds significantly slower than that of the dominant wave [*Plant*, 1997; *Plant et al.*, 1999a, 1999b]. At the short fetches, millimeter-length bound waves were shown to be parasitic capillary waves [*Plant et al.*, 1999b]. In this paper, we report experiments carried out in a large wind-wave tank in

0148-0227/04/2004JC002342$09.00

Figure 1. Inside of the wind-wave tank at Luminy, France. At the far end of the tank is the carriage holding the wind- and wave-monitoring equipment.

Luminy, Marseille, France, in the summer and fall of 2000. Coherent microwave and acoustic systems with wavelengths within 10% of each other were set up to view the same spot on the water surface at the same time, incidence angles, and azimuth angles with respect to the wind. The measurements confirmed that both mean Doppler shifts (Doppler offsets) and cross sections could be explained by a bound wave/free wave model. The bound waves were found to travel at the dominant wave phase speed at fetches near 7 m but at the phase speed of a wave half as long as the dominant wave at fetches near 26 m. The millimeter-length bound waves responsible for backscattering 8 mm radiation were shown not to be parasitic capillary waves at fetches near 26 m. Free wave spectral densities were found to drop rapidly to zero with increasing azimuth angle, becoming virtually undetectable at 55° to the wind. Bound waves were found to decrease much more slowly, or not at all, with azimuth angle. The sum of bound and free wave spectral densities deduced from fitting data to model was close to past measurements of total short-wave spectral densities at various azimuth angles and wind speeds.

2. Description of Tank and Experiment

[4] Figure 1 shows the inside of the wind-wave tank at Luminy. The tank is 40 m long and 3 m wide. During our experiments the water was 0.9 m deep, and the air channel was 1.5 m high. Wind was measured with a combination of Pitot tubes and hot film anemometers and reached a maximum speed of ~12.5 m/s at the center of the air channel. A capacitance wave gauge yielded omnidirectional variance spectra of surface wave height. Table 1 gives wind, wave, and fetch conditions during the runs reported here.

[5] K_u (14 GHz, 2 cm wavelength) and K_a (35 GHz, 8 mm wavelength) band, continuous wave, coherent microwave systems were operated from above the tank looking through a large window covered with polyethylene. The systems were both dual polarized so that vertical transmit and receive polarization (VV) and horizontal transmit and receive polarization (HH) returns could be obtained simultaneously. Henceforth we will refer to these as the radars. Coherent, pulsed acoustic systems at 70 kHz (2 cm wavelength) and 190 kHz (8 mm wavelength) were operated from below the water. Henceforth we will call these systems the sonars. Figure 2a shows the K_a band radar above the tank, while Figure 2b shows the 190 kHz sonar under the water. We arranged the radar and sonar so that they always viewed the same spot on the water surface at the same incidence and azimuth angles. This was ensured by floating a metal sphere on the water surface and maximizing the return from the sphere to both systems. A schematic side view of the experimental arrangement is presented in Figure 2c.

[6] Figure 3 is a top view of the tank showing the locations of the centers of the various surface areas illuminated during the course of the experiment at various incidence and azimuth angles. The nominal fetch at the center of the circular pattern of illuminated spots was 27 m but could be reduced to 8.2 m by covering the upwind water surface with a plastic sheet. The fetch at the measured spot varied somewhat as the incidence and azimuth angles varied. The distance from the centerline to the outer illuminated spots (50° incidence angle) was 1.7 m; the distance to the inner spot (30° incidence angle) was 0.4 m. So, looking upwind, the actual fetch of the illuminated spot varied from 25.3 to 26.6 m (from 6.5 to 7.8 m with the plastic sheet) depending upon the incidence angle. Most runs were made with the water uncovered, although a few runs were made at the shorter fetch near the end of the experiments. In the calculations of the dominant wavelength used in the modeling, the ±6% variations in fetch for

Table 1. Wind, Wave, and Fetch Parameters Used During These Experiments[a]

U at 50 cm, m/s	U at 12 cm, m/s	u_*, cm/s	H_s, cm	λ_p, cm	c_p, cm/s
		25 m Fetch			
3.02	2.59	8.8	0.54	14.2	48.6
4.09	3.48	12.7	1.01	23.5	61.8
5.14	4.32	17.2	1.48	32.5	72.2
6.19	5.21	20.2	2.09	35.2	75.1
8.20	6.75	31.4	2.88	53.8	91.7
10.36	8.32	45.9	3.86	59.4	95.7
12.55	9.65	64.6	5.41	76.8	106.9
		8.0 m Fetch			
2.99	2.65	7.9	0.01	3.12	27.2
4.02	3.61	10.3	0.20	4.76	31.2
5.07	4.52	13.3	0.50	10.2	42.5
6.10	5.38	16.6	0.72	14.2	49.4
8.14	6.96	26.2	1.24	21.4	60.0
10.28	8.69	35.1	1.72	27.6	67.6
12.46	10.19	50.0	2.54	39.7	79.7

[a] U, wind speed, given at two heights; u_*, friction velocity; H_s, significant wave height; λ_p, the dominant wavelength; and c_p, the phase speed of the dominant wave as given by *Plant and Wright* [1980] for the measured u_* and λ_p.

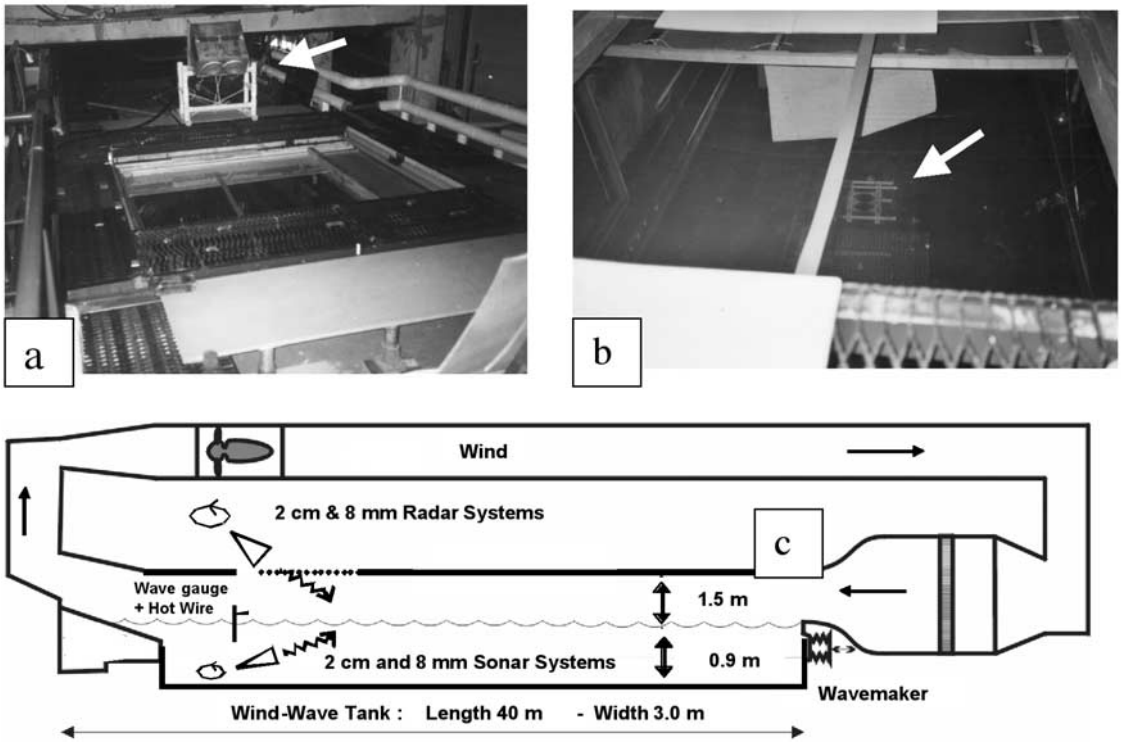

Figure 2. (a) K_a band (8 mm) radar (arrow) looking down through the polyethylene window in the top of the air channel. The K_u band (2 cm) radar was operated from the same position. (b) The 190 kHz (8 mm) sonar (arrow) shown under water, as viewed through the window in the top of the air channel. The 70 kHz (2 cm) sonar was also operated from this position. (c) Schematic side view of the experimental arrangement.

different incidence and azimuth angles have been taken into account.

3. Doppler Spectra

[7] Doppler spectra of the backscattered signal for 2 cm wavelength radiation at a 40° incidence angle are shown in Figures 4 and 5 for various wind speeds. Note that zero indicates that the received microwave and acoustic frequencies have no Doppler shift. Figure 4 shows Doppler spectra measured looking into the wind (azimuth angle is 0°). HH radar spectra are dash-dotted lines, VV radar spectra are dashed lines, and sonar spectra are solid lines. The vertical lines indicate the expected frequency for a Bragg resonant surface wave moving at its own phase speed (solid line) and at the phase speed of the dominant wave (dashed line). Phase speeds were calculated including wind effects as given by *Plant and Wright* [1980]. Note that the single peak seen in the sonar Doppler spectrum is at the frequency of a wave traveling close to the free wave phase speed in most cases. In contrast, both radar Doppler spectra exhibit two strong peaks for the midrange of wind speeds. These peaks are near the frequencies expected for surface waves traveling at the free wave phase speed and at the dominant wave phase speed as indicated by their approximate correspondence with the vertical lines. Note, however, that the higher-frequency peaks appear to be a bit below the frequency that would be expected if they indeed traveled at the dominant wave phase speed.

[8] The bottom right panel of Figure 4 summarizes the behavior of the cross sections as a function of wind friction velocity. In this paper, cross sections are normalized cross sections expressed in the radar convention. These are equivalent to sonar scattering strengths times 4π [*Dahl et al.*, 1997]. Note that both HH and VV radar cross sections exceed those of the sonar by large amounts.

[9] Figure 5 is similar to Figure 4 except that the antennas and transducers are directed downwind (azimuth angle is 180°). Now, in contrast to Figure 4, the microwave Doppler spectra generally show a single peak near the free wave phase speed, while the acoustic spectrum shows a single peak near the dominant wave phase speed with the hint of a second peak near the free wave phase speed. Furthermore, the sonar cross sections are now generally equal to or greater than the HH polarized radar cross sections.

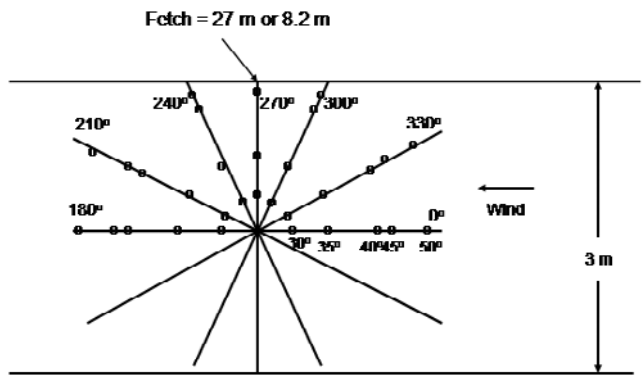

Figure 3. Plan view of experimental arrangement showing the locations of the centers of the illuminated areas.

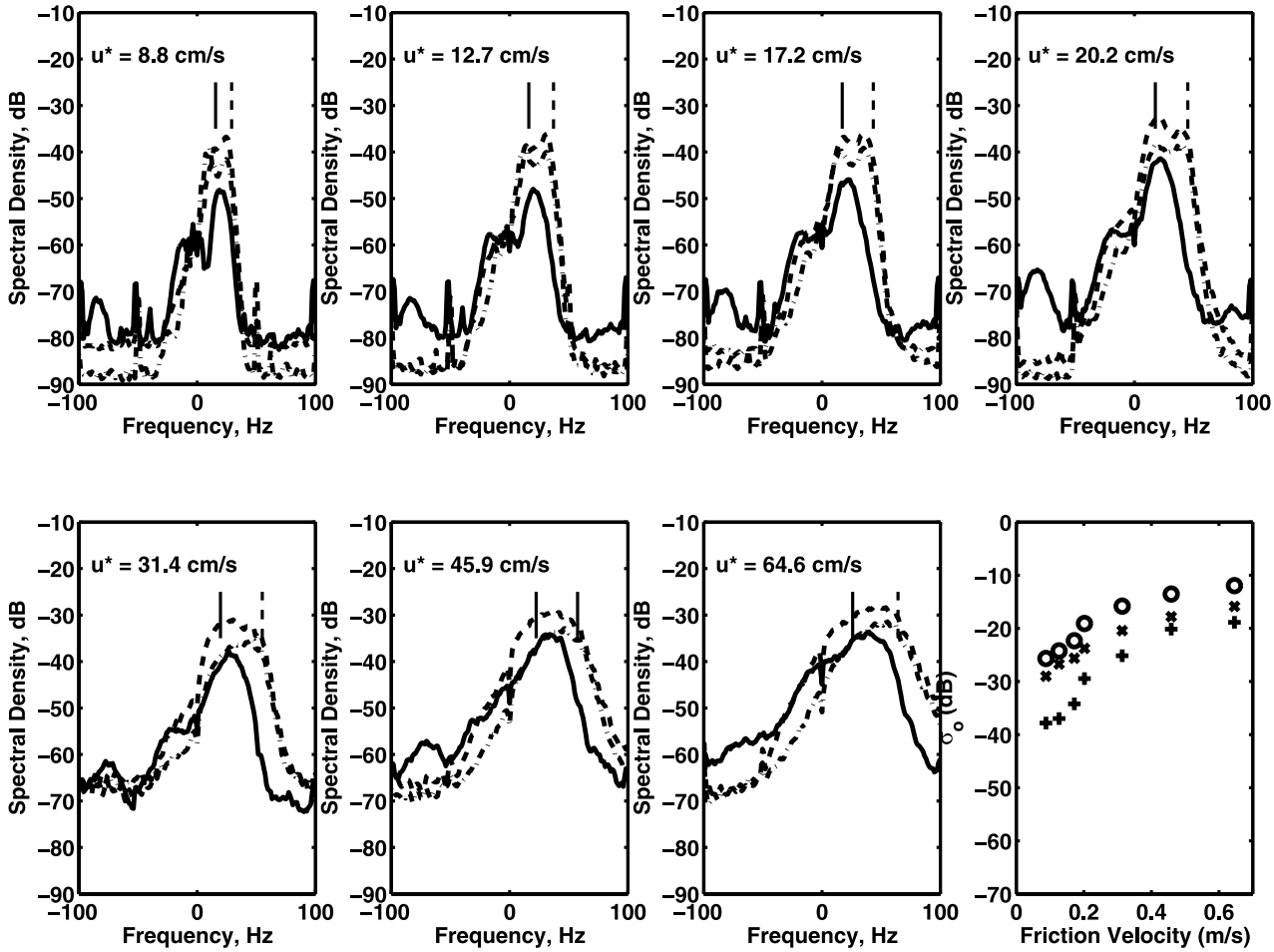

Figure 4. Doppler spectra of backscattered 2 cm wavelength radiation at an incidence angle of 40° and a fetch of 25.9 m looking upwind for the two microwave polarizations (dashed lines and circles indicate vertical transmit and receive polarization (VV); dash-dotted lines and crosses indicate horizontal transmit and receive polarization (HH)) and for the acoustic signal (solid lines and pluses). The solid vertical line is the expected frequency of a Bragg wave traveling at its own phase speed; the dashed vertical line is the expected frequency of a Bragg wave traveling at the dominant wave phase speed. The bottom right panel shows cross section versus friction velocity.

[10] This behavior is easy to explain on a bound wave/free wave model if the bound waves reside primarily on the forward, or leeward, face of their parent wave, are tilted by the underlying long wave, and are moving with the long wave. If this is the case, then the microwave systems will have a smaller local incidence angle at the location of the bound waves than the acoustic system when both are looking upwind. Since smaller incidence angles lead to stronger backscatter, the bound waves should show up more strongly in the microwave spectra in this case, as observed. When looking downwind, the situation is reversed, again, as observed. Note that this picture of the rough water surface fits a gentle spilling breaking process.

4. Comparison of Long- and Short-Fetch Measurements

[11] We made similar microwave and acoustic measurements at 2 cm and 8 mm in a short wind-wave tank at the University of Washington (UW) in 1998 [*Plant et al.*, 1999b]. Comparison of the measurements made in the Luminy tank in 2000 with those previous measurements shows the consistency of the measurements and also indicates some differences in behavior between long and short fetches. Figure 6 compares measurements made using 2 cm wavelengths in the UW tank at a 5 m fetch and an incidence angle of 50° with both radar and sonar looking upwind (solid lines), with similar measurements made in Luminy at long (dashed lines) and short (dotted lines) fetches. Measured cross sections (Figure 6a) were nearly the same at all fetches, to within ~3 dB, at all wind speeds. In contrast, Doppler offsets, that is, the first moments of the Doppler spectra (Figure 6b), increase with fetch at most wind speeds. Furthermore, the increase in Doppler offset is greater from 5.0 to 6.5 m fetch than it is from 6.5 to 25.5 m.

[12] Figure 7 shows cross sections and Doppler offsets measured at 8 mm wavelength and a 50° incidence angle looking upwind in the UW tank and at long fetch in the

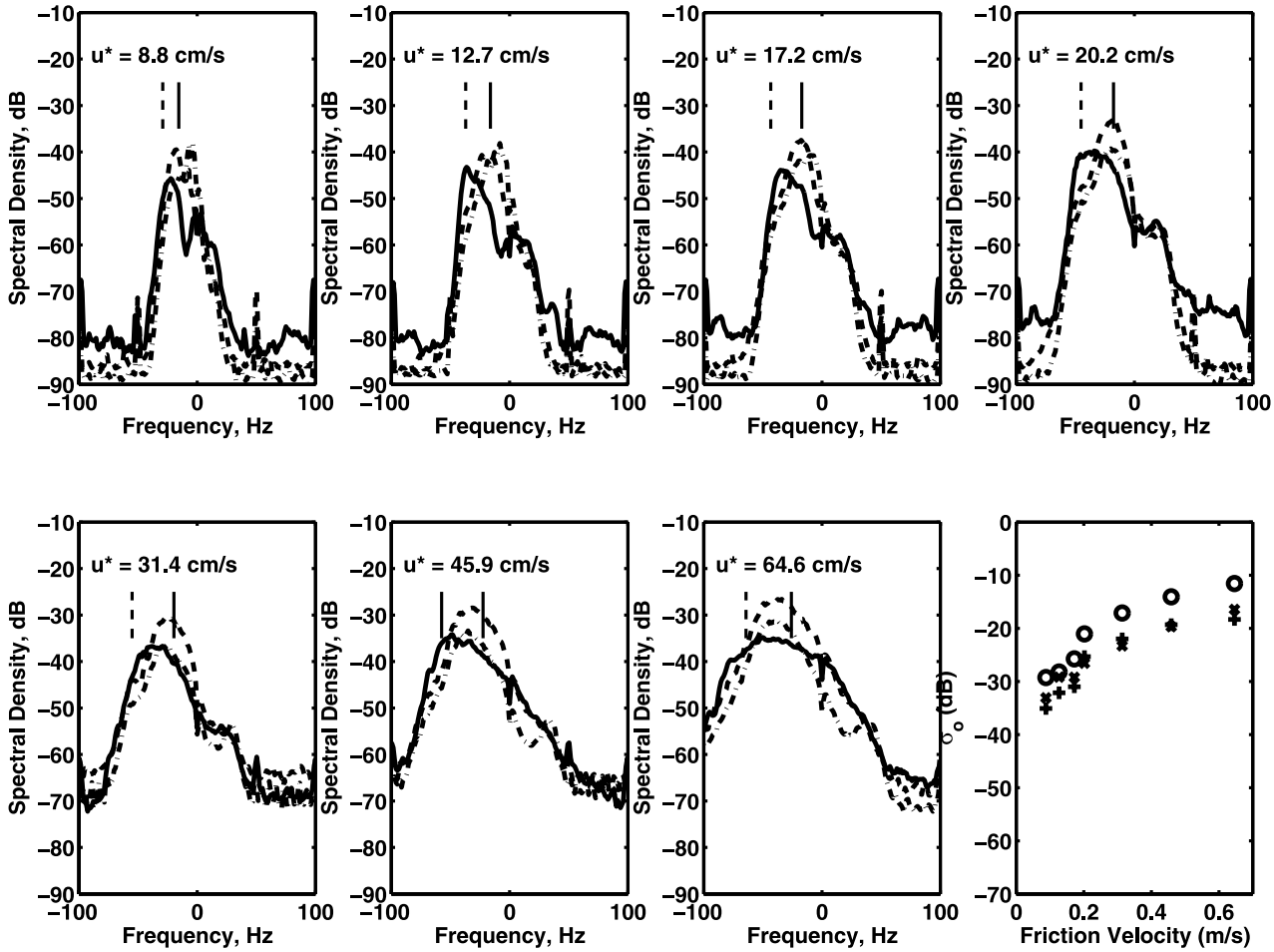

Figure 5. Same as Figure 4 but for antennas and transducers looking downwind.

Luminy tank; unfortunately, no short-fetch data were collected at this wavelength in Luminy. For this wavelength the cross sections are different at the two fetches, the most dramatic difference being the peak in cross section at a friction velocity of ~0.18 m/s in the short-fetch data. We have identified the backscatter at this wind speed, fetch, and wavelength to be a result of scattering from parasitic capillary waves [*Plant et al.*, 1999b]. A reasonable conclusion from Figure 7 is that this is no longer the case at the longer fetch. Instead, the scatter appears to be due to other types of bound waves that exist at this fetch. We will return to this point in section 8. Doppler offsets once again show an increase with fetch at all wind speeds.

5. Bound Wave/Free Wave Model of Cross Sections and First Moments

[13] We have discussed our bound wave/free wave model of microwave backscatter from wind-roughened water surfaces many times in the past, so we will be brief here. The model postulates that roughness is created by long, wind-generated waves on the leeward side of their crests as shown in Figure 8. These are bound waves; they may be parasitic capillaries or breaking wave products. Since they are localized on the long wave, they have a mean tilt in the downwind direction and are moving, if not exactly at the long-wave phase speed, then very near it. Not shown in Figure 8 are the free waves, which we picture as being generated directly by the wind, covering the surface outside of bound wave regions, and traveling at their own intrinsic phase speed, as modified by the long-wave orbital velocity. We assume that the turbulence due to the bound waves in front of the long-wave crest damps the free waves there. This is particularly valid at high winds where air flow separation at the crest of the dominant wave induces a reattachment of the air flow downwind far from the crest just behind the sheltered zone where the tangential stress drops. Therefore the mean free wave slope is not zero but must be in the opposite direction to that of the bound waves in order that the overall surface slope be zero (or at least very small, since setup occurs, especially in tanks).

[14] Backscatter to microwave or acoustic systems is calculated according to this model by simply adding scattering due to bound waves to the standard Bragg/composite surface scattering theory [*Wright*, 1968; *Bass et al.*, 1968]. The resulting normalized cross section (cross section divided by illuminated area) is then given by

$$\sigma_o = \sigma_c + \sigma_b,$$

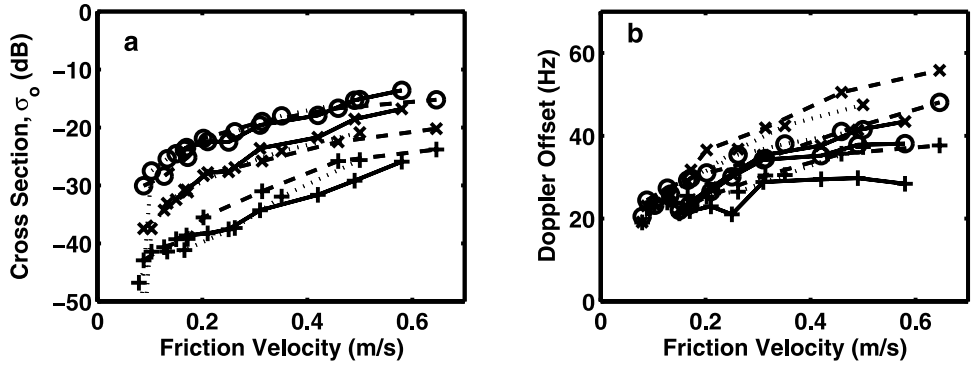

Figure 6. (a) Two centimeter cross sections versus friction velocity. (b) Two centimeter Doppler offsets versus friction velocity. Data were taken with 2 cm wavelength radiation and a 50° incidence angle with both radar and sonar directed upwind. Pluses indicate sonar, crosses indicate radar HH, and circles indicate radar VV. Data at 5 m fetch (solid lines) were collected in 1998 in the University of Washington wind-wave tank; data at 6.5 m (dotted lines) and 25.5 m fetches (dashed lines) were collected in 2000 in the large wind-wave tank in Luminy, Marseille, France.

where the composite surface cross section σ_c and the bound wave cross section σ_b are given by

$$\sigma_c = \iint \sigma_B(\theta_o + \gamma, \alpha) P_f P(\gamma, \alpha|f) \mathrm{d}\gamma \mathrm{d}\alpha$$

$$\sigma_b = \iint \sigma_B(\theta_o + \gamma, \alpha) P_b P(\gamma, \alpha|b) \mathrm{d}\gamma \mathrm{d}\alpha,$$

where θ_o is the nominal incidence angle, (γ, α) are the long-wave slopes in and perpendicular to the plane of incidence, respectively, P_f is the probability of finding free waves, P_b is the probability of finding bound waves, and $P(\gamma, \alpha|x)$ is the probability distribution of a wave of type x, either free or bound. σ_B is the standard Bragg scattering cross section

$$\sigma_B = 16\pi k_o^4 |g(\theta_o + \gamma, \alpha)|^2 F_x[2k_o \sin(\theta_o + \gamma), 0],$$

where g is a function of the dielectric constant and local incidence and tilt angles, k_o is the microwave number, and F_x is the wave height variance spectrum of either free or bound waves evaluated at $[2k_o\sin(\theta_o + \gamma), 0]$. More details, including the forms of g for VV and HH polarization, are given by *Plant et al.* [1999a]. Values of g for acoustic scattering are the same as those for HH electromagnetic Bragg scattering from a perfectly conducting surface.

[15] Doppler offsets may be calculated in this model as the weighted sum of Doppler shifts of scattering from free and bound waves, either of which may be calculated from

$$f_x = 2V \sin\theta_o/\lambda,$$

where x is either f for free waves or b for bound waves. For free waves, V is the intrinsic phase speed of the Bragg wave, $\lambda_B = \lambda/(2\sin\theta_o)$. For bound waves, V is near the speed of propagation of the parent wave. Here λ is either the microwave or acoustic wavelength ($=2\pi/k_o$). The total Doppler offset is therefore given by

$$f_d = \left(\sigma_c f_f + \sigma_b f_b\right)/\sigma_o.$$

[16] Some observations about this model are in order. First, if a significant difference exists between the sonar cross section and the HH radar cross section, then tilting of the scatterers is indicated. This means that maxima of the

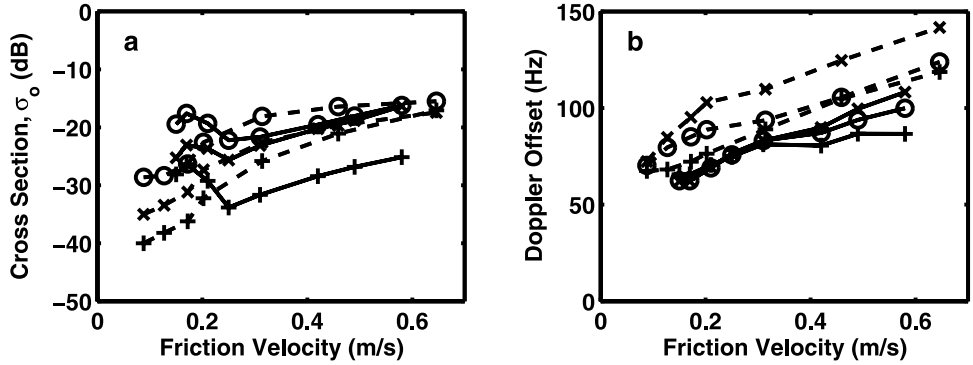

Figure 7. Same as Figure 6 but at 8 mm. No data were taken at short fetches in the Luminy tank at this wavelength.

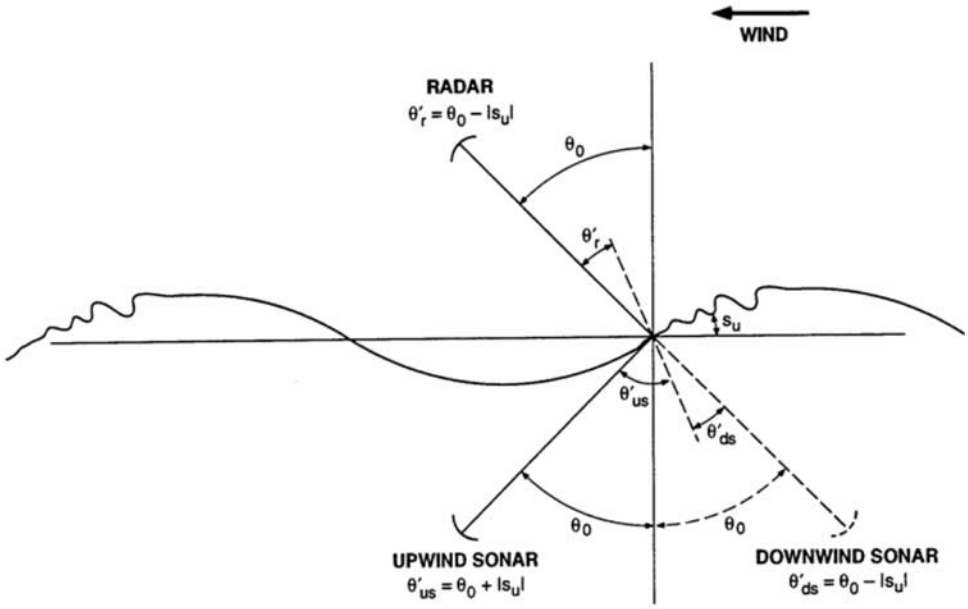

Figure 8. Bound wave/free wave model showing the difference in local incidence angle when bound waves are viewed from above and below the water surface. Free waves are assumed to exist everywhere outside of the region of bound waves on the leeward face of the long wave.

conditional probabilities P are not at $\gamma = 0$. If γ_b is the mean bound wave tilt, then the mean free wave tilt is

$$\gamma_f = -P_b\gamma_b/P_f$$

in order to give the overall surface zero slope. Second, the mean spectral density of either bound or free waves is given by

$$\langle F_x \rangle = F_x P_x.$$

Third, in the model either changing the tilt or changing the mean spectral density will change the resulting cross section. Therefore σ_b may be kept constant if $\langle F_x \rangle$ is changed to compensate for a change in tilt. Recall that the tilt of the bound waves must be set at a value that will yield the correct ratio of HH radar to sonar cross sections. Finally, the region where bound waves exist could be too rough to allow Bragg scattering to be a good approximation there. However, in section 6, data will be compared with the model on the basis of Bragg scattering, and the agreement is generally good.

[17] Both the long-wave slopes in and perpendicular to the plane of incidence affect the value of the computed cross section. Since in these experiments we looked at various azimuth angles with respect to the wind and we assume that the bound wave tilt is all in the wind direction, the effective tilts in and perpendicular to the plane of incidence change as the azimuth angle changes. Also, we assume that the mean motion of the bound waves is in the direction of the wind so the component of the bound wave mean velocity in the direction of the azimuth angle is used in computing the bound wave Doppler offset.

6. Comparison of Data and Model

[18] This bound wave/free wave scattering model was implemented in MATLAB, and results were computed by adjusting free and bound wave spectral densities as a function of wave number to fit the data as well as possible. Values of the mean square slopes of free and bound waves are required for the calculation of the conditional probabilities P, which were assumed to be Gaussian; these and the values of P_b were obtained from *Plant et al.* [1999a]. Mean tilts (slope angles) of the bound waves were adjusted from those given by *Plant et al.* [1999a] as required to fit the data, and free wave tilts were obtained from the equations of section 5. P_f was obtained from P_b: $P_f = 1 - P_b$.

[19] Figure 9 shows the fit of the data at 2 cm to the model in the case of the radar and sonar both directed upwind for a fetch of 25.5 m. The fits to the cross sections, while not perfect, are reasonably good. Importantly, if neither free nor bound waves exhibited a mean tilt, the large difference in the values of the acoustic and HH microwave cross sections could not be explained. The predicted Doppler offsets fit somewhat less well since they are very sensitive to the relative cross sections of bound and free waves. The best fits are given by the solid, uppermost dashed, and dash-dotted lines which are predictions based on the assumption that the bound waves travel at the phase speed of a wave half as long as the dominant wave. Figure 9 shows that the agreement with data is not as good if the bound waves are assumed to travel at the dominant wave phase speed or at their own phase speed (the dotted and bottommost dashed lines are HH Doppler offsets for these cases).

[20] Figure 10 shows the same comparisons at 8 mm, again with radar and sonar both directed upwind. In this case, the fit of the cross sections is somewhat worse than at 2 cm, particularly for VV polarization, but in general, the fit is still within 3 dB of the data. Doppler offsets once again suggest that the bound waves move at the phase speed of a wave half as long as the dominant wave.

[21] Because of the width of the tank at Luminy the angular dependence of the free and bound waves could be

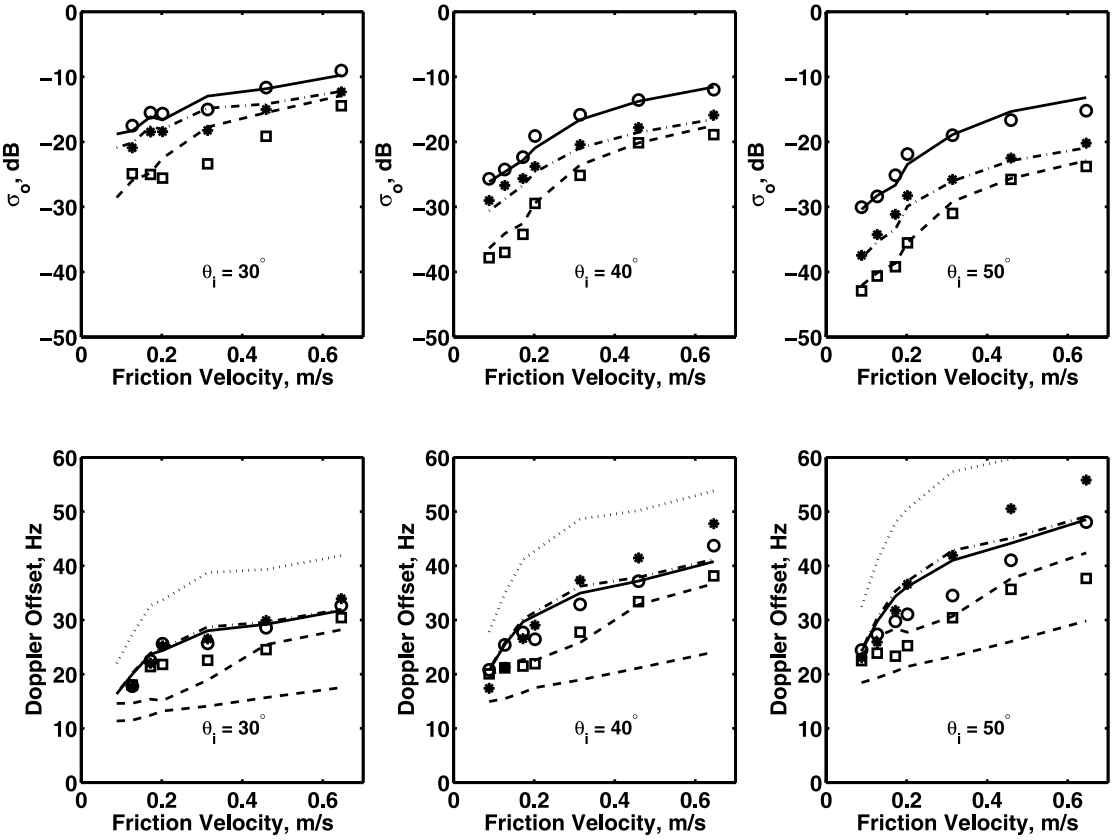

Figure 9. (top) Microwave and acoustic cross sections measured at 2 cm and various incidence angles versus friction velocity for fetches near 26 m. (bottom) Two centimeter Doppler offsets versus friction velocity. Both microwave and acoustic systems are directed upwind. Lines are best fits to the bound wave/free wave model. The dotted line in the bottom panels is the predicted Doppler offset for HH microwave backscatter if the bound waves move at the dominant wave phase speed. The bottommost dashed line is the HH offset if the bound waves move at their intrinsic phase speed. Other lines are predicted on the basis of bound waves moving at the phase speed of a wave half as long as the dominant wave. Dash-dotted lines and asterisks indicate HH, solid lines and circles indicate VV, and dashed lines (uppermost in bottom panels) and squares indicate sonar.

determined from the microwave and acoustic data but only at the lower incidence angles. Figure 11 shows comparisons between 2 cm data and the model similar to those shown in Figures 9 and 10 but for an azimuth angle 55° from the wind direction. Again, the fits of the model to the cross sections are rather good, and those for the Doppler offsets indicate that the bound waves are not moving at either the dominant wave phase speed or their own intrinsic phase speed. During the experiments we had assumed that the azimuth angle for this run was 60° from the wind direction, but the observed Doppler shifts could not be fit with this azimuth angle. Reduction of the angle by 5° produced the good fits shown in Figure 11.

[22] At this azimuth angle the fit of cross sections and Doppler offsets to the model could only be produced by setting bound wave spectral densities much larger than those of free waves. The two types of waves produced different effects because their mean tilts are constrained by the data at other azimuth angles. Thus the data indicate that short waves traveling at large angles to the wind are bound waves resulting from the crosswind irregularities of roughness regions associated with breaking. Here we are referring to spilling, often microscale, breaking that does not have significant air entrainment [see *Jessup et al.*, 1997].

[23] The observation that the bound waves do not travel at the phase speed of the dominant wave for fetches near 26 m is intriguing because our previous work at 5, 10, and 12.5 m fetches has shown that they do travel with the dominant wave at those fetches [*Plant et al.*, 1999a, 1999b]. On the other hand, the primary breaking waves on the ocean are definitely not the dominant waves [*Plant*, 1997; *Melville and Matusov*, 2002]. To see whether the results in the Luminy tank were consistent with our previous measurements, we fit the model to the 2 cm data taken at 6.5 m fetch. The results are shown in Figure 12. In this case, the measured Doppler offsets were best fit by assuming that the bound waves traveled at the dominant wave phase speed in agreement with our previous measurements.

[24] We collected data at seven different azimuth angles, as shown in Figure 3. The data collected looking directly across the tank were not valid at any incidence angle because of backscatter from the side. At the other azimuth angles we were able to fit the data to the model as well as shown in the examples above. An exception was when the

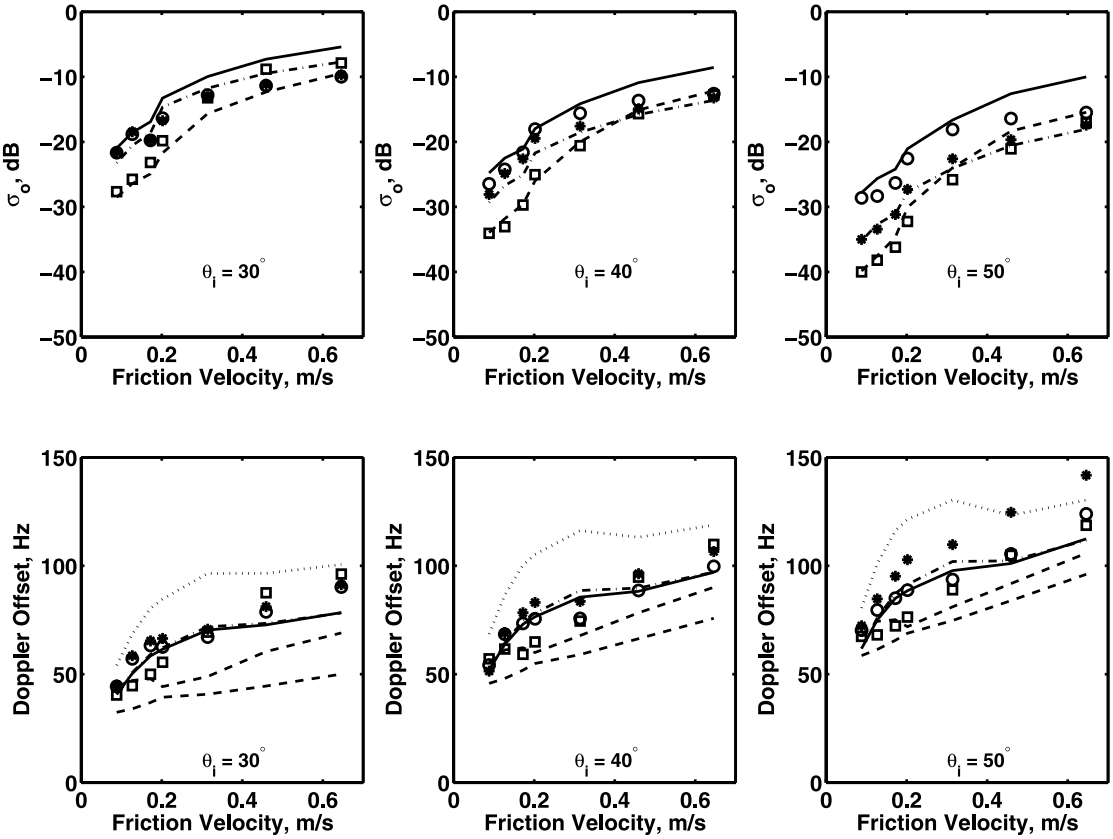

Figure 10. Same as Figure 9 but for 8 mm incident radiation.

microwave and acoustic systems were pointed directly downwind. In this case the fit deteriorated somewhat, probably because of reflections of the microwave signals from the carriage on which the wind- and wave-measuring equipment was mounted (see Figure 1). Several conclusions were supported by data at all incidence angles: Bound and free waves have a mean tilt, bound waves travel at the dominant wave phase speed at short fetches but at the speed of a wave half as long at fetches near 26 m, and short waves traveling at large angles to the wind are not produced directly by the wind but by the breaking of longer waves.

7. Short-Wave Spectral Densities

[25] The primary parameters adjusted to produce the fits between the model and data shown in section 6 were the mean spectral densities of the free and bound waves. However, several other parameters were necessary in the model in addition to these spectral densities. Mean square slopes and the probabilities of finding free and bound waves used here were the same as those used by *Plant et al.* [1999a]. Figure 13 shows the mean tilt angles of the bound waves used to fit the data at the two different fetches in these experiments. Also shown in Figure 13 are the mean bound wave tilt angles found in our previous experiments [*Plant et al.*, 1999a, 1999b]. These slopes are negative to indicate that they are slopes on the leeward side of the long-wave crest where the height of the long wave is decreasing in the direction of travel.

[26] Using these slopes and the other parameters obtained in past experiments, we were able to derive mean spectral densities of free and bound waves individually at various azimuth angles and wind speeds. Their sum is the total short-wave spectral density. We specified these spectral densities with a piecewise continuous function, each piece of which was given by $\langle F_x \rangle = C_x k^{-n}$. Spectral densities of the curvature spectrum $B(k) = k^4 \langle F_x \rangle$ that produced the best fits to the data for waves traveling in the wind direction at various friction velocities are shown in Figure 14. Total spectral densities measured by other investigators are also shown in Figure 14; our values appear to be somewhat lower than the other measurements.

[27] Because we used a range of incidence angles, two different radiation wavelengths, and both radar and sonar in these experiments, we were able to derive spectral densities over a range of wave numbers from about 170 to 1400 rad/m. The regions covered by 8 mm and 2 cm incident radiation are enclosed by the vertical dashed and solid lines, respectively, in Figure 14. In the area of overlap between the two regions, between 400 and 500 rad/m, the same spectral densities had to fit the backscatter at both 8 mm and 2 cm. It is interesting to note that bound waves dominate the short-wave spectrum at high wave numbers at low wind speeds but free waves become dominant at these wave numbers at the higher wind speeds.

[28] Figure 15 is the same as Figure 14 except that it is for an azimuth angle 55° away from the wind direction. *Hara et al.* [1997] did not give values at this azimuth angle, but *Jähne and Riemer* [1990] gave values at 60° from the wind;

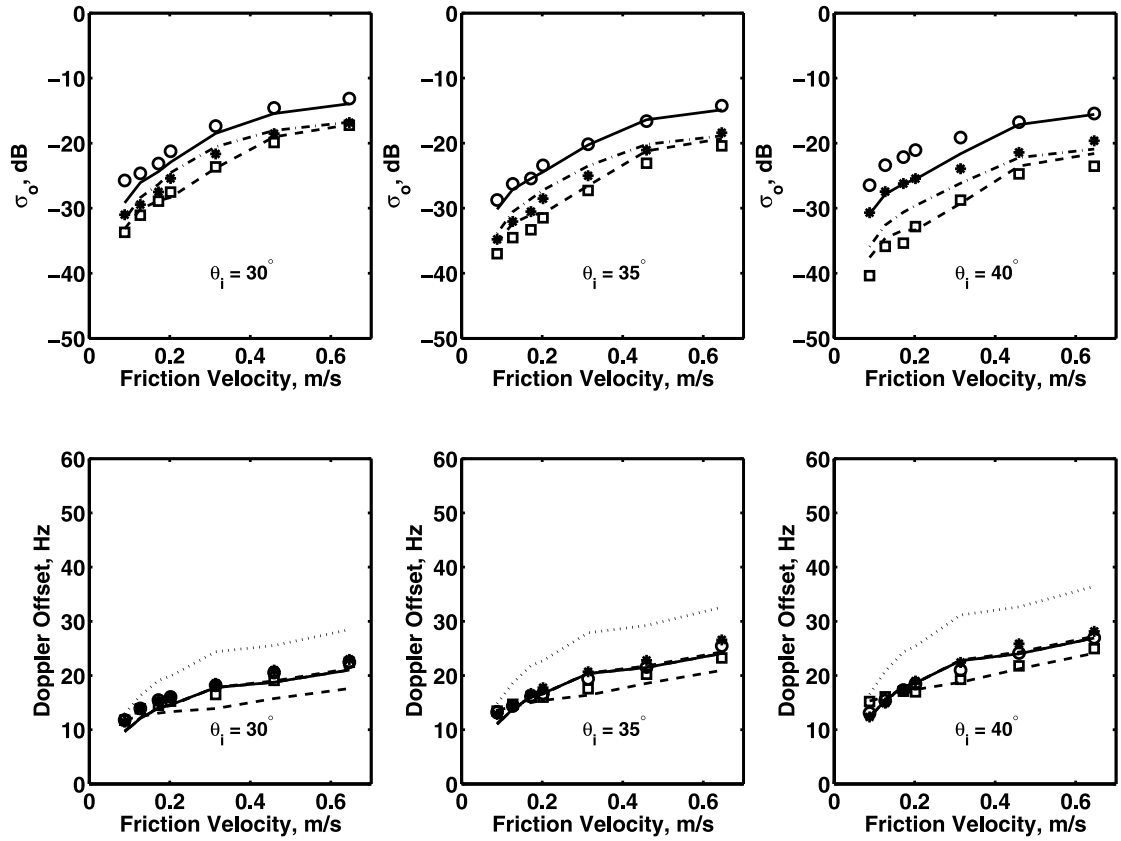

Figure 11. Same as Figure 9 but at an azimuth angle 55° from the wind direction. Incidence angles above 40° are not shown because they were contaminated by backscatter from the side of the tank.

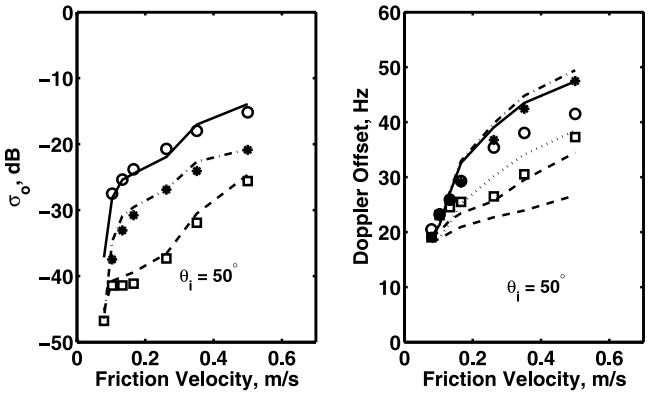

Figure 12. Cross sections and Doppler offsets measured with 2 cm wavelength incident radiation at a 50° incidence angle looking upwind with a fetch of 6.5 m. Symbols are the same as in Figure 9, but the lines indicate the following: (left) Dash-dotted line indicates HH; the solid line indicates VV; and the dashed line indicates sonar. (right) Bottommost dashed line indicates HH, assuming that bound waves move at their own phase speed; the dotted line indicates HH, assuming that bound waves move at the phase speed of a wave half as long as the dominant wave; the dash-dotted line indicates HH; solid line indicates VV; and the topmost dashed line indicates sonar, all assuming that bound waves move at the dominant wave phase speed.

these are shown in Figure 15. Jähne and Riemer's total spectral densities are larger than ours at all but the highest wave numbers. Thus our measurements imply a narrower azimuthal spread for the short waves than do Jähne and Riemer's. As mentioned above, our measurements also indicate that bound waves dominate the short-wave spectrum at this azimuth angle. In fact, the spectral levels of the free waves shown in Figure 15 really only indicate upper limits; any free wave spectral densities less than those shown will have a negligible effect on the backscatter. Note that the dash-dotted line for the bound waves is difficult to see in many parts of Figure 15 because the solid line for the total spectral density is plotted over it.

[29] We summarize the azimuthal dependence of the spectral densities of free, bound, and total short waves found in this study as shown in Figure 16. Total short-wave spectral densities usually decrease with increasing azimuth angle except at the higher wave numbers and lowest wind speed where they remain essentially flat out to 55°. The reason for this latter behavior is not entirely clear but may be simply that the uncertainty in our determination of spectral density is larger than any decrease with azimuth angle at this wind speed. The striking behavior is that the free wave spectral density decreases much faster than that of the bound waves with azimuth angle. This indicates that short waves directly generated by the wind have a much narrower azimuthal spread than do short waves that are generated by longer waves.

8. Discussion and Conclusion

[30] We have observed the properties of microwave and acoustic backscatter from a wind-roughened water surface in a large wind-wave tank using 2 cm and 8 mm wavelength radiation. We have shown that the data can be fit by a model that postulates that short surface waves are produced both directly by the wind (free waves) and indirectly by longer wind waves (bound waves). Three properties of the received signals required that such a model be used rather than a model in which all waves are directly generated by the wind. The first property is that Doppler spectra obtained at moderate wind speeds with antennas and transducers looking in the same horizontal direction exhibit two peaks in either the microwave or acoustic spectrum but never in both. The spectrum exhibiting two peaks switches from microwave to acoustic as the azimuth angle varies from upwind to downwind. The second property is that HH microwave cross sections differ, in general, from acoustic cross sections by much more than expected from a simple wind-wave model. This indicates that some of the scatterers have a mean tilt so that the local incidence angle at their location is different for radiation incident on the surface from above than from below. The third property is that first moments of the Doppler spectra, or Doppler offsets, show that some short waves on the surface move much faster than their expected phase speed.

[31] The speed at which the bound waves move was found to be the phase speed of the dominant wave in the tank at fetches near 7 m but was found to decrease to the phase speed of the first spatial harmonic of the dominant wave at fetches near 26 m. This is in line with past observations that show that bound waves move at the dominant wave phase speed when the fetch is below

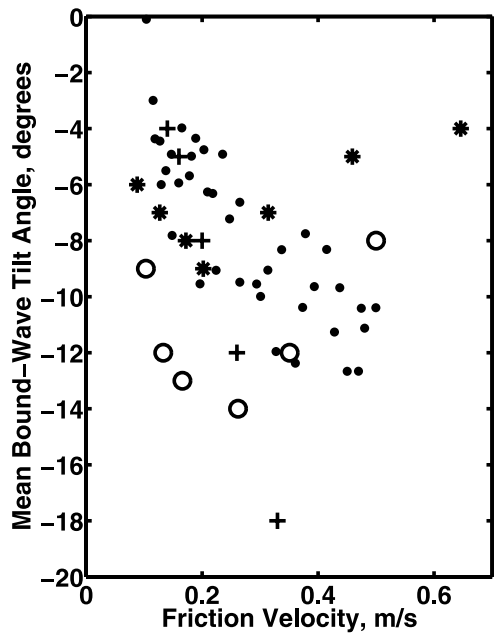

Figure 13. Mean bound wave slopes measured in these experiments and in previous experiments. Asterisks indicate 6.5–7.8 m fetch (this study), circles indicate 25.3–26.6 m fetch (this study), pluses indicate 5.0 m fetch [*Plant et al.*, 1999b], and dots indicate 14.3 m fetch [*Plant et al.*, 1999a]. All values were derived from microwave and acoustic measurements except the dots, which came from direct measurements using a laser slope gauge.

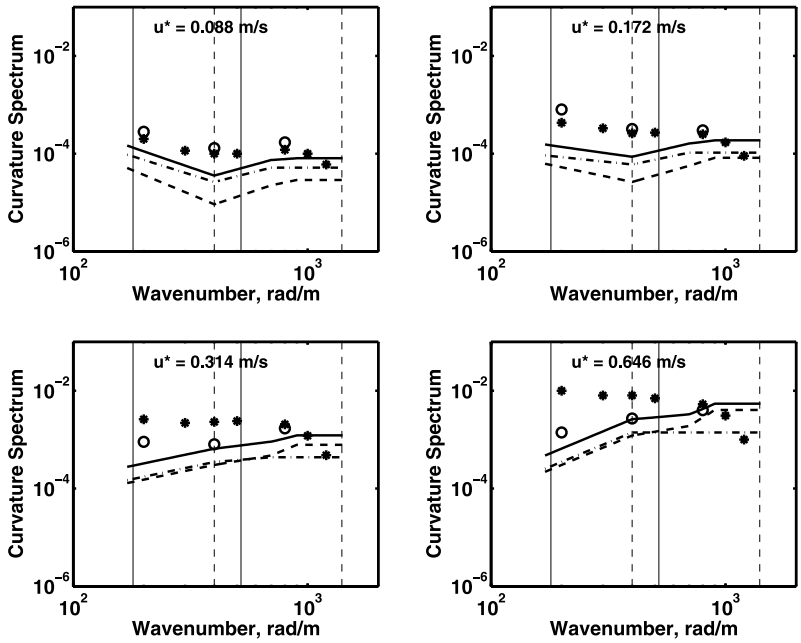

Figure 14. Curvature spectrum versus wave number at various friction velocities for waves propagating in the wind direction and at a fetch near 26 m. The dashed line is the free wave spectral density from this experiment, the dash-dotted line is the bound wave spectral density, and the solid line is the total short-wave spectral density determined in this experiment. Vertical solid lines enclose the region interrogated with 2 cm wavelength radiation; vertical dashed lines enclose the region interrogated with 8 mm wavelength radiation. The asterisks indicate values of the total short-wave spectral density from *Jähne and Riemer* [1990] at a fetch of 100 m and friction velocities of 0.073, 0.14, 0.27, and 0.72 m/s. The circles are the corresponding values from *Hara et al.* [1997] at a fetch of 13 m and friction velocities of 0.10, 0.19, 0.32, and 0.61 m/s.

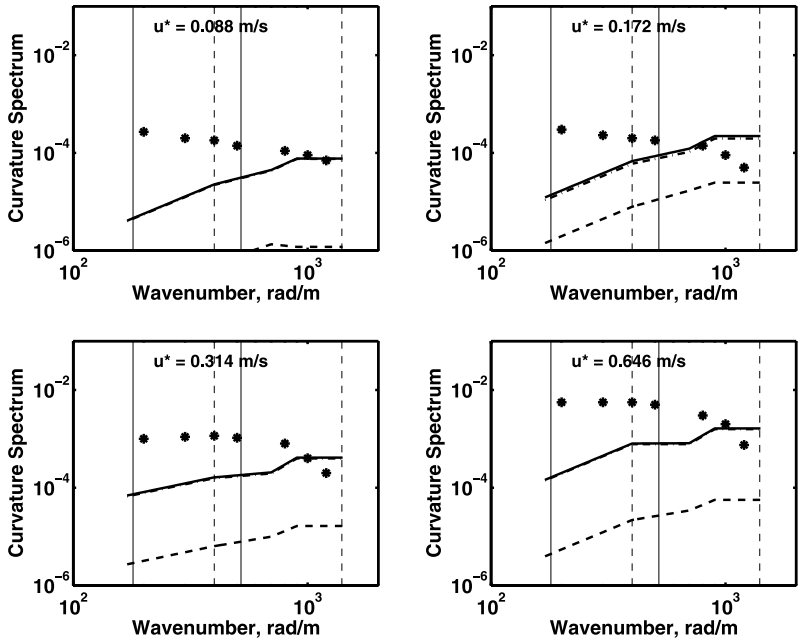

Figure 15. Same as Figure 14 except at a 55° azimuth angle to the wind. *Jähne and Riemer*'s [1990] values (the asterisks) are at 60° to the wind. Free wave spectral densities shown in Figure 15 should be considered an upper limit rather than a measured value.

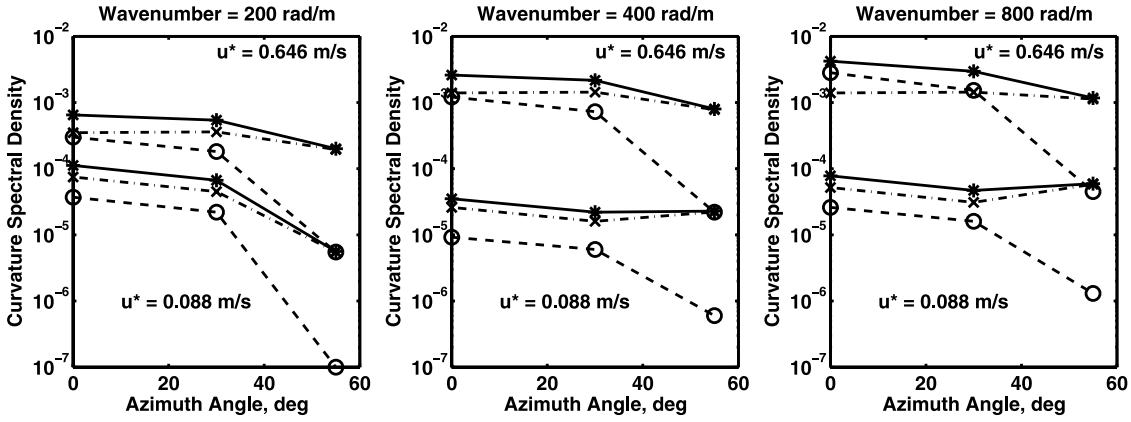

Figure 16. Curvature spectra of free, bound, and total short waves versus azimuth angle with respect to the wind, as determined in the present experiment for 3.2, 1.6, and 0.8 cm wavelengths, respectively. Asterisks and solid lines are the total short-wave spectral densities, crosses and dash-dotted lines are bound waves, and circles and dashed lines are free waves.

~15 m but that bound waves on the ocean move much more slowly than the dominant wave phase speed [*Plant*, 1997; *Plant et al.*, 1999a, 1999b]. *Melville and Matusov* [2002] also showed that whitecaps on the ocean, which account for a small fraction of the bound waves, travel at speeds well below those of the dominant waves.

[32] The dependence of the backscatter on azimuth angle with respect to the wind shows that spectral densities of free waves, i.e., those directly generated by the wind, fall rapidly for large azimuth angles. Bound waves, on the other hand, fall much more slowly with increasing azimuth angle, sometimes even appearing isotropic in our measurements. This conclusion came from both the cross-section data and the Doppler offset data. Cross sections at large azimuth angles could not be fit with significant free wave spectral densities if the mean slopes of the bound and free waves were kept at the levels that fit data taken at smaller azimuth angles. Doppler offsets corresponded closely to the component of the bound wave velocity along the observed azimuthal direction and did not generally correspond to the expected phase speed of a free wave. These observations lead us to conclude that short surface waves on wind-roughened water surfaces that travel at large angles to the wind are manifestations of lateral roughness variations in the turbulent regions of breaking waves.

[33] Finally, the present observations show that the bound, millimeter-length waves responsible for backscattering 8 mm incident radiation do not move at their intrinsic phase speed at long fetches. Previously, in short fetch situations we found that these waves did move at their intrinsic phase speed, which was also the dominant wave phase speed [*Plant et al.*, 1999a]. This led us to identify the scatterers at these short fetches as parasitic capillary waves. Since at the longer fetches of this experiment the speed of these bound waves is clearly different from their intrinsic phase speed, we conclude that they are primarily turbulence associated with spilling breaking rather than parasitic capillaries. This probably accounts for the much higher cross sections found for 8 mm wavelength radiation at low winds for short fetches than for long fetches (see Figure 7). It implies that spectral densities of parasitic capillary waves are larger than those associated with breaking turbulence. The fact that the bound, centimeter-length surface waves that backscatter 2 cm wavelength radiation never move at their intrinsic phase speed shows that they are never parasitic capillary waves. This is because at these wavelengths it is not possible to match the speeds of gravity and capillary waves. This probably accounts for the similarity of cross sections for 2 cm wavelength radiation at low winds for long and short fetches (see Figure 6). The results of these experiments confirm our earlier findings that backscatter from wind-roughened water surfaces cannot be accurately explained without including effects of parasitic capillary waves and the regions of roughness associated with spilling or microscale breaking waves.

[34] **Acknowledgments.** The authors would like to thank the technicians of the IRPHE, Alain Laurence, Bertrand Zucchini, and Raymond Vaudo, for their valuable assistance during the experiments. We also thank William Keller, who constructed both the microwave and acoustic systems and prepared them for these experiments, and Ken Hayes, who developed the data acquisition software.

References

Bass, F. G., I. M. Fuks, A. I. Kalmykov, I. E. Ostrovsky, and A. D. Rosenberg (1968), Very high frequency radiowave scattering by a disturbed sea surface. Part I: Scattering from a slightly disturbed boundary, *IEEE Trans. Antennas Propag.*, *AP-16*(5), 554–559.

Dahl, P. H., W. J. Plant, B. Nutzel, A. Schmidt, H. Herwig, and E. A. Terray (1997), Simultaneous acoustic and microwave backscattering from the sea surface, *J. Acoust. Soc. Am.*, *101*(5), 2583–2595.

Fedorov, A. V., W. K. Melville, and A. Rozenberg (1998), An experimental and numerical study of parasitic capillary waves, *Phys. Fluids*, *10*, 1315–1323.

Hara, T., E. J. Bock, and M. Donelan (1997), Frequency-wavenumber spectrum of wind-generated gravity-capillary waves, *J. Geophys. Res.*, *102*(C1), 1061–1072.

Jähne, B., and K. S. Riemer (1990), Two-dimensional wave number spectra of small-scale water surface waves, *J. Geophys. Res.*, *95*(C7), 11,531–11,546.

Jessup, A. T., C. J. Zappa, M. R. Loewen, and V. Hesany (1997), Infrared remote sensing of breaking waves, *Nature*, *385*, 52–55.

Melville, W. K., and P. Matusov (2002), Distribution of breaking waves at the ocean surface, *Nature*, *417*, 58–63.

Plant, W. J. (1997), A model for microwave Doppler sea return at high incidence angles: Bragg scattering from bound, tilted waves, *J. Geophys. Res.*, *102*(C9), 21,131–21,146.

Plant, W. J. (2003a), A new interpretation of sea-surface slope probability density functions, *J. Geophys. Res.*, *108*(C9), 3295, doi:10.1029/2003JC001870.

Plant, W. J. (2003b), Microwave sea return at moderate to high incidence angles, *Waves Random Media*, *13*(4), 339–354, doi:10.1088/0959–7174/13/4/009.

Plant, W. J., and J. W. Wright (1980), Phase speeds of upwind and downwind traveling short gravity waves, *J. Geophys. Res.*, *85*(C6), 3304–3310.

Plant, W. J., W. C. Keller, V. Hesany, T. Hara, E. Bock, and M. Donelan (1999a), Bound waves and Bragg scattering in a wind-wave tank, *J. Geophys. Res.*, *104*(C2), 3243–3263.

Plant, W. J., P. H. Dahl, and W. C. Keller (1999b), Microwave and acoustic scattering from parasitic capillary waves, *J. Geophys. Res.*, *104*(C11), 25,853–25,866.

Rozenberg, A. D., M. J. Ritter, and W. K. Melville (1999), Free and bound capillary waves as microwave scatterers: Laboratory studies, *IEEE Trans. Geosci. Remote Sens.*, *37*(2), 1052–1065.

Wright, J. W. (1968), A new model for sea clutter, *IEEE Trans. Antennas Propag.*, *AP-16*(2), 217–223.

H. Branger and J.-P. Giovanangeli, Institut de Recherche sur les Phénomènes Hors Équilibre, Centre National de la Recherche Scientifique, F-13288 Marseille Cedex 9, France.

P. H. Dahl and W. J. Plant, Applied Physics Laboratory, University of Washington, 1013 NE 40th Street, Seattle, WA 98105-6698, USA. (plant@apl.washington.edu)